Photocatalytically Green Synthesis of H_2O_2 by Using 2-Ethyl-9,10-anthraquinone as an Electron Condenser

Dandan Zhang, Gangqiang Xu, Tao Chen, Feng Chen*
Key Laboratory for Advanced Materials and Institute of Fine Chemicals, East China University of Science and Technology, 130 Meilong Road, Shanghai, 200237, China

1. Synthesis of the Pt/P25 catalyst.

Pt nanoclusters were loaded onto TiO_2 (P25, Degussa) particles by a typical photoreduction method. The reaction solution consisted of 80 mL CH_3OH and 20 mL distilled water with an addition of 10 mL 1.0 g/L $H_2PtCl_6 \cdot 6H_2O$ (Sinopharm Chemicals, >99.9%) solution. 1.0 g P25 TiO_2 was dispersed in the solution in a quartz flask. The flask was then photoirradiated using a Xe lamp (PLS-SXE300) for 3.0 h under magnetic stirring. The Pt clusters were formed from $PtCl_6^{2-}$ by reacting with the photogenerated electrons on the surface of TiO_2. The obtained light graypowders were then washed several times with water, vacuum dried at 60 ^oC and labeled as Pt/P25.

The content of Pt in the as-prepared Pt/P25 catalyst was detected by XPS and gave a value of 0.4 wt%.

2. Photocatalytic H_2O_2 synthesis.

2-ethyl-9,10-anthraquinone (EAQ, Sinopharm Chemicals, 98%) was dissolved in 100 mL CH_3OH (Sinopharm Chemicals, >99.5%) which was deaerated in advance by ultrasonicating and vacuuming. Pt/P25 catalyst (0.20 g) was then added into the

solution under N_2 protection in a quartz flask. The suspension was photoirradiated using a Xe lamp (PLS-SXE300) under magnetic stirring and N_2 protection. At a regular interval, a volume of 3-4 mL suspension was sampled, centrifuged to remove the photocatalyst, and then air bubbled 5 min to obtain H_2O_2 from H_2EAQ (Eq. S1).

$$H_2EAQ + O_2 \rightarrow EAQ + H_2O_2 \qquad (S1)$$

3. Determination of H_2O_2.

H_2O_2 concentration was determined by an iodometric titration. 10 mL 200 g/L NaCl aqueous solution and 1.0 mL of 0.5 M HCl were mixed in a 25 mL colorimetrical cylinder. The cylinder was put in a water bath to control the temperature of the solution at 25 ^oC. Then 2.0 mL sample solution, 1.0 mL starch solution (10.0 g/L) and 2.0 mL KI solution (5.0 g/L) were added into the cylinder. The solution was immediately diluted to 25 mL with distilled water. Wait 20 min to coloration and detect the absorbance of the solution at the wavelength of 565 nm (Shimadzu UV-2600).

4. Hydrogen evolution.

0.2 g Pt/P25 sample was dispersed in 100 mL methanol aqueous solution (methanol/water = 20/80 (v/v)). The photocatalytic reaction was carried out in a quartz cell connected to a closed gas circulation and evacuation system. After the system was vacuumed, the suspension was irradiated by a 300 W Xe lamp (PLS-SXE300) under magnetic stirring. The (H_2) gas generated was sampled every 30 min

and then analyzed by an in-situ gas chromatograph (GC7890 II, Techcomp, 5 Å molecular sieve column, TCD).

5. By-products analysis with HPLC and LC-MS.

By-products of the reaction were analyzed by a HPLC instrument (LC-20A, Shimadzu) and a LC-MS system (LCMS-IT-TOF, Shimadzu). For the LC part, InertSustain C18 column (4.6 × 250 mm, 5 μm) was selected as the chromatographic column; mobile phase condition: A/B = H_2O/methanol; 0-1 min, 60% B; 1-10 min, gradient change from 60% B to 82%B; 10-18 min, 82% B; 18.01-28 min, 60% B, flow rate 1.0 mL/min. DAD detector was used to trace the substances.

For the MS part, atmospheric pressure chemical ionization (APCI) was selected as the ion source, and a high resolution TOF detector was used. Ion source interface voltage: 4.5 kV, -3.5 kV; Nebulizer gas: N_2, 1.5 L/min; Drying gas: N_2, 10 L/min; Interface temperature: 300 ^oC; CDL: 280 ^oC; Heating block: 280 ^oC; Detector voltage: 1.4 kV.

6. Mechanism of H_2O_2 generation.

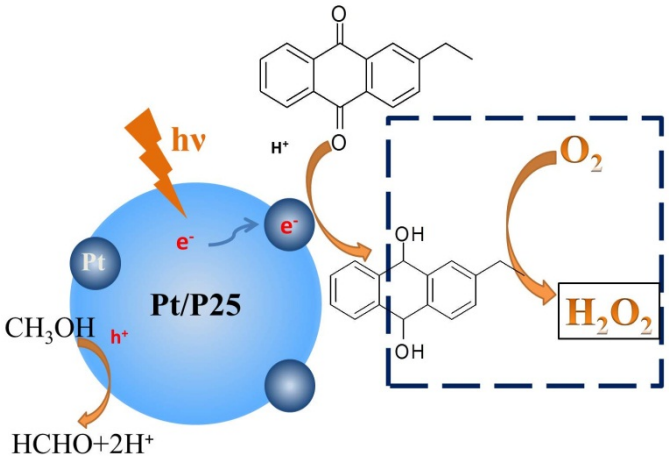

Figure S1. Mechanism of H_2O_2 generation with Pt/P25 in photocatalytic reaction

The H_2O_2 is generated via a TiO_2 photocatalysis-related process. Briefly, the absorption of UV irradiation induces an electron excitation in TiO_2, which results in the generation of an electron at conductive band and a hole at valence band of TiO_2. The photogenerated electron will transfer to the surface deposited Pt clusters, where the photogenerated electron would react with and reduce the EAQ molecules to give H_2EAQ, while the photogenerated hole is captured with hole scavenger, methanol.

When the photocatalytic process is over, the photocatalyst, Pt/P25, can be removed from the H_2EAQ solution. The production of H_2O_2 then can be easily achieved by air bubbling. As we know, the reaction of oxygen with H_2EAQ leads to the quick formation of H_2O_2.

7. XRD patterns of P25 and Pt/P25 composite.

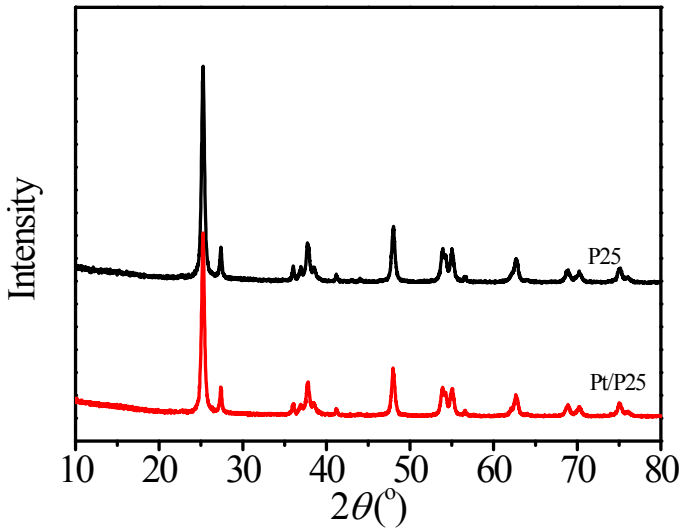

Figure S2. XRD patterns of P25 and Pt/P25

Pt/P25 has a just similar XRD pattern as that of P25, which is composed of anatase and rutile (rutile/anatase =20/80). The Pt XRD signals are absence in the Figure S2, which may be ascribed to the very low content of Pt in the Pt/P25 composite.

8. TEM observation of P25 and Pt/P25 composite.

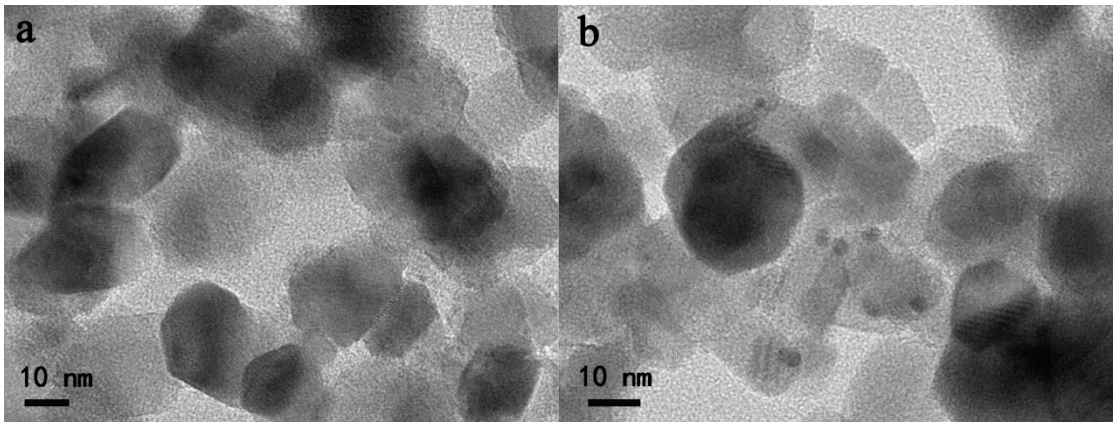

Figure S3. TEM images of (a) bare P25 and (b) Pt/P25

As shown in Fig. S3, P25 material is composed of TiO_2 grains with a size range of

20-30 nm. As for TEM image of Pt/P25, many small black dots appear, which should be ascribed to deposited Pt clusters in the composite.

8. UV-visible DRS spectrum of Pt/P25 and absorption spectrum of EAQ.

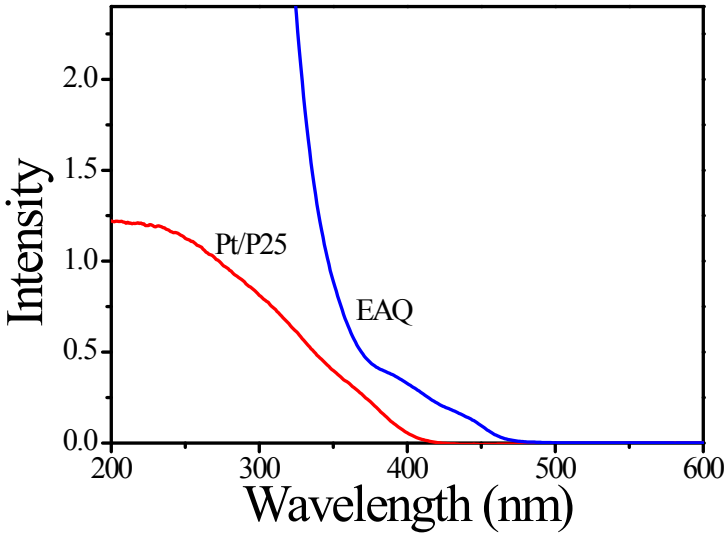

Figure S4. UV-visible DRS spectrum of Pt/P25 and absorption spectrum of EAQ (0.25 g/L in methanol).

After the Pt deposition, the Pt/P25 composite extends its light absorption from UV to 406 nm as shown in Fig. S4. Meanwhile, EAQ exhibits significant light absorption in the visible region and has a absorption edge of 471 nm. The absorption region of Pt/P25 is overlapped with that of EAQ, and therefore, a much high concentration of EAQ seems adverse to the practical photo-absorption of Pt/P25 photocatalyst.

9. Reduction kinetics of EAQ and the corresponding reaction rate constants.

The reduction of EAQ to the H_2EAQ is considered as a fast reversible reaction combined with a slow continuous reaction, as shown in Eq. S2.

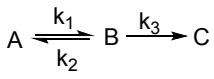

(S2)

Here A refers to EAQ, B refers to H_2EAQ and C refers to by-products. The k_1 and k_3 are apparent zero-order reaction rate constants and k_2 is an apparent first-order reaction rate constant. Therefore, the temporal concentration of H_2EAQ (C_B) can be predicted according to the initial EAQ concentration (C_0) with the following equation (Eq. S3).

$$C_B = k_1/k_2 \times C_0\text{^}0.5 \times (1\text{-}exp(\text{-}k_2 t))\text{-}k_3 C_0 t \qquad (S3)$$

Consequently, the corresponding k_1, k_2 and k_3 values for the reduction of EAQ were calculated by fitting the experimental data (Fig. 1B) and are listed in Table S1.

Table S1. Calculated k_1, k_2 and k_3 values for the reduction of EAQ and the optimal reaction time for H_2EAQ production.

EAQ (mM)	k_1 (mM h^{-1})	k_2 (h^{-1})	k_3 (mM h^{-1})	Optical reaction time (h)
4.2	3.42	2.38	0.06	1.4
8.5	1.55	0.42	0.10	3.9
12.7	1.26	0.38	0.03	6.5
16.9	0.95	0.30	0.02	8.2
25.4	0.61	0.25	0.01	10.0

10. Identification of by-products with HPLC and LC-MS.

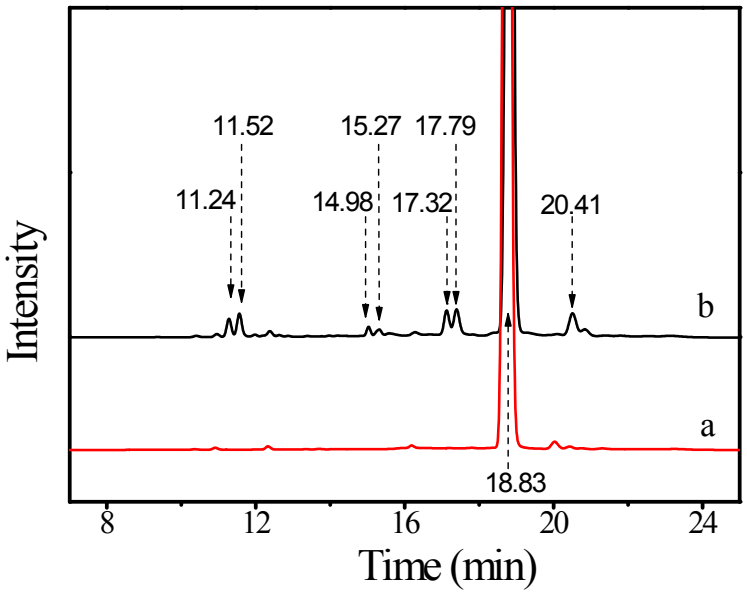

Figure S5. HPLC spectra of EAQ solutions (4.0 g/L) (a) before and (b) after 7 h irradiation.

The by-products as well as the EAQ were analyzed with the HPLC instrument. Fig. S5 shows the HPLC spectra of EAQ solution before and after 7 h light irradiation. Besides the EAQ, several chemical substances appear in the HPLC spectra. By using the LC-MS technique, the chemical structures of above substances were identified to be oxo-EAQ1 (11.24 min), oxo-EAQ2 (11.52 min), 2-ethyl-9-anthranol (14.98 min), 2-ethyl-10-anthranol (15.27 min), EAN1 (17.32 min), EAN2 (17.79 min), EAQ (18.83 min), and an isomer of EAQ (20.41 min, the exact chemical structure has not been identified).

The MS spectra of above substances are shown as follow.

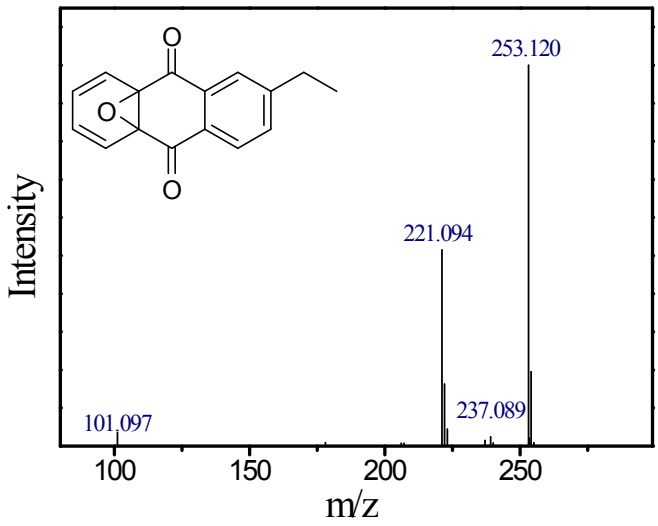

Figure S6. MS spectrum of the substance at retention time of 11.24 min.

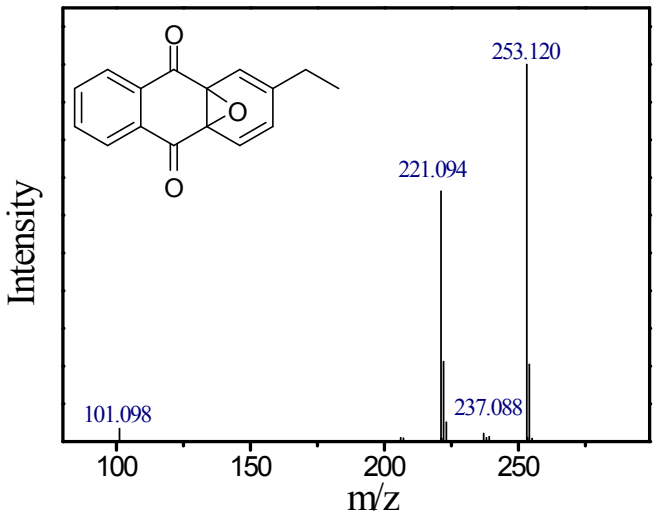

Figure S7. MS spectrum of the substance at retention time of 11.52 min.

MS spectra of the substances at retention time of 11.24 min and 11.52 min are shown in Figures S6&S7. Both substances show a $[M+H]^+$ signal at m/z 253.120 as the major peak. According to isotopic information and their exact masses, the molecular formulas of these two substances are concluded as $C_{16}H_{12}O_3$ (oxo-EAQ1, 11.24 min) and $C_{16}H_{12}O_3$ (oxo-EAQ2, 11.52 min), respectively. The chemical

structures of oxo-EAQ1 and oxo-EAQ2 are correspondingly presented in the Figures S6&S7.

The proposal formation pathways for oxo-EAQ1 and oxo-EAQ2 are presented in Scheme S1. The reduction of EAQ with the photoexcited electron induces to the formation of a 2-ethyl-semi-hydroanthraquinone intermediate (semi-HEAQ), which is unstable and possibly hydrolysis to form an oxo-2-ethyl-hydroanthraquinone radical (oxo-H_2EAQ radical). Then the oxo-H_2EAQ radical disproportionates to give an electron and transform itself into the oxo-2-ethylhydroanthraquinone (oxo-H_2EAQ). When the solution is oxygen bubbled, the oxo-H_2EAQ reacts with oxygen to produce oxo-EAQ and H_2O_2.

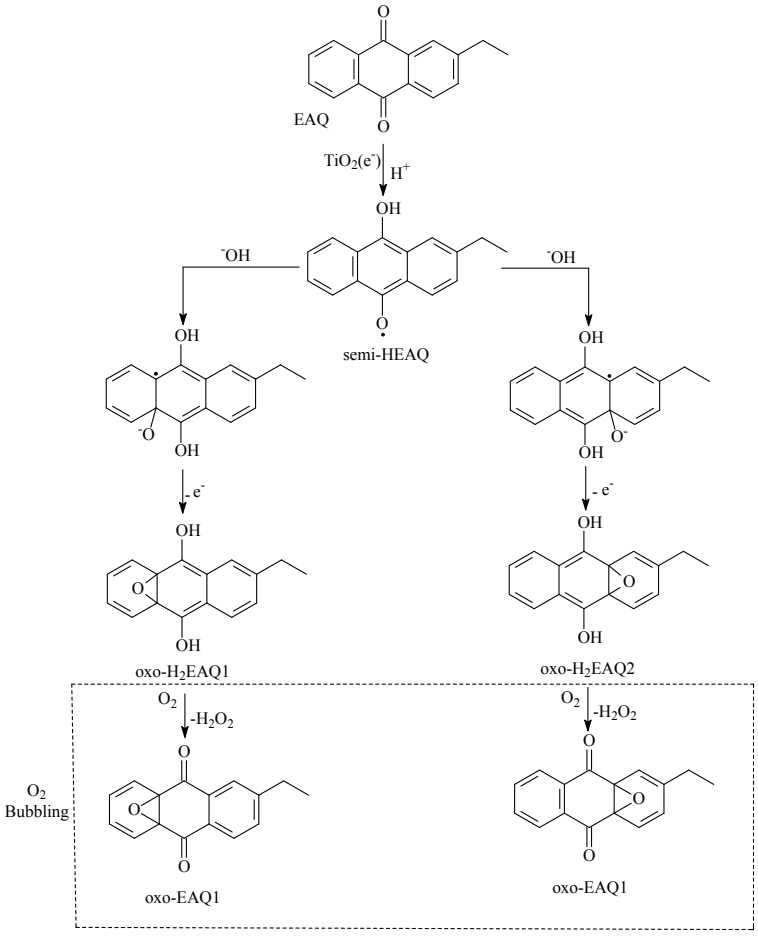

Scheme S1. The proposal formation pathways for oxo-EAQ1 and oxo-EAQ2

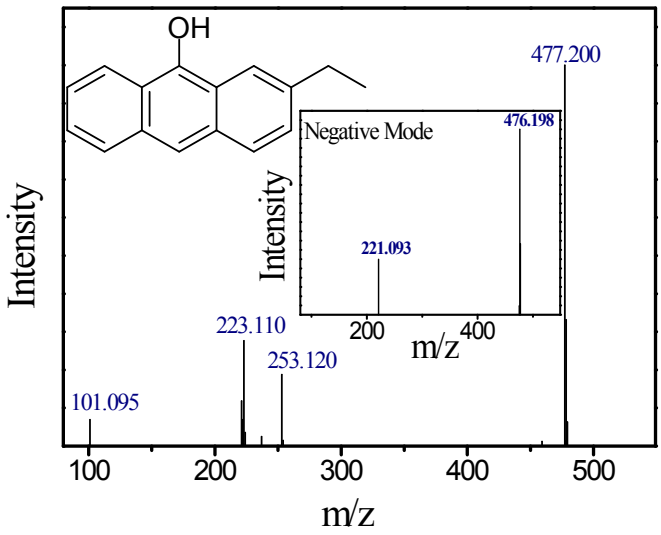

Figure S8. MS spectrum of the substance at retention time of 14.98 min.

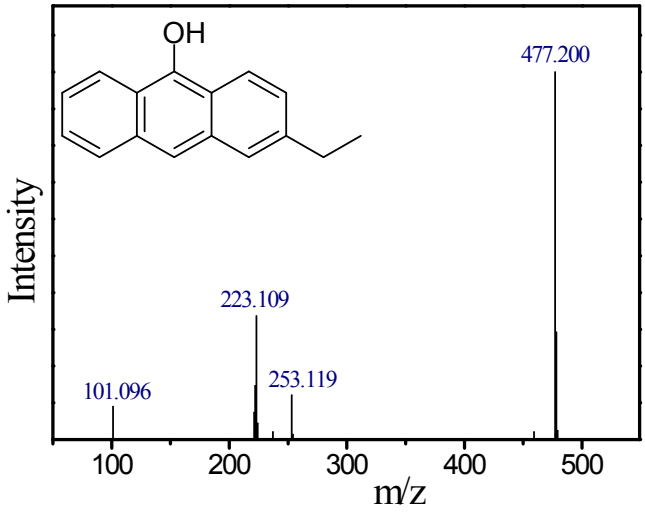

Figure S9. MS spectrum of the substance at retention time of 15.27 min

MS spectra of the substances at retention time of 14.98 min and 15.27 min are shown in Figures S8&S9. Both substances show a $[M+H]^+$ signal at m/z 223.110 (or 223.109) as the major peak. The inset in Fig. S8 shows that the molecule has a $[M-H]^-$ signal at m/z 221.093 in negative mode. The signals at m/z 477.200 is due to the solvated dimer $[2M+CH_3OH_2]^+$[S1-S6]. The signal at m/z 253 can be ascribed to the

background noise as no corresponding signal can be observed in negative mode. According to isotopic information and their exact masses, the molecular formulas of these two substances are concluded as $C_{16}H_{14}O$ (2-ethyl-9-anthranol, 14.98 min) and $C_{16}H_{14}O$ (2-ethyl-10-anthranol, 15.27 min), respectively. The chemical structures of 2-ethyl-9-anthranol and 2-ethyl-10-anthranal are correspondingly presented in the Figures S8&S9.

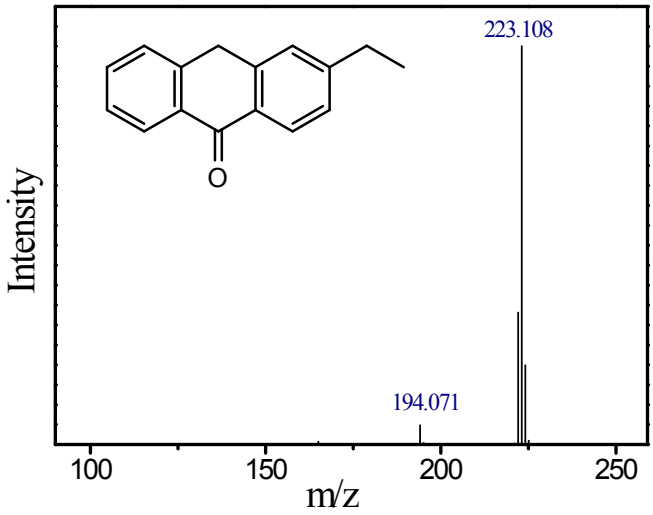

Figure S10. MS spectrum of the substance at retention time of 17.32 min

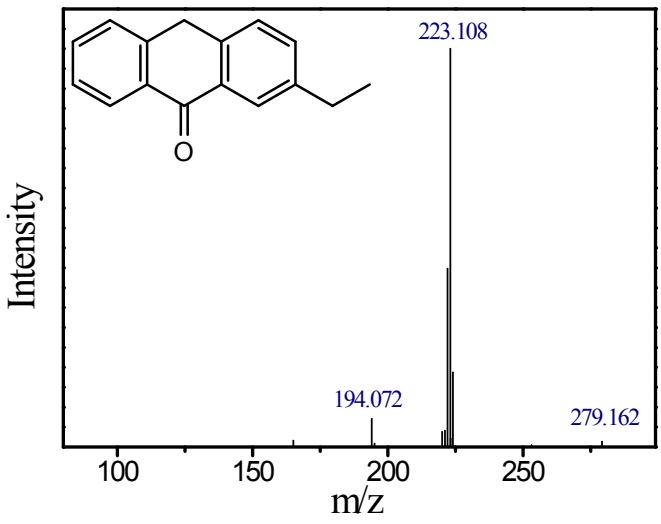

Figure S11. MS spectrum of the substance at retention time of 17.79 min

MS spectra of the substances at retention time of 17.32 min and 17.79 min are shown in Figures S10&S11. Both substances show a $[M+H]^+$ signal at m/z 223.108 as the major peak. According to isotopic information and their exact masses, the molecular formulas of these two substances are concluded as $C_{16}H_{14}O$ (2-ethyl-10H-9-anthranone, 17.32 min) and $C_{16}H_{14}O$ (2-ethyl-9H-10-anthranone, 17.79 min), respectively. The chemical structures of 2-ethyl-10H-9-anthranone and 2-ethyl-9H-10-anthranone are correspondingly presented in the Figures S10&S11.

It is proposed that the four anthranol & anthranone substances are produced due to the over-reduction of H_2EAQ. The possible generation pathway of 2-ethyl-10-anthranol and 2-ethyl-9H-10-anthranone is shown in Scheme S2.

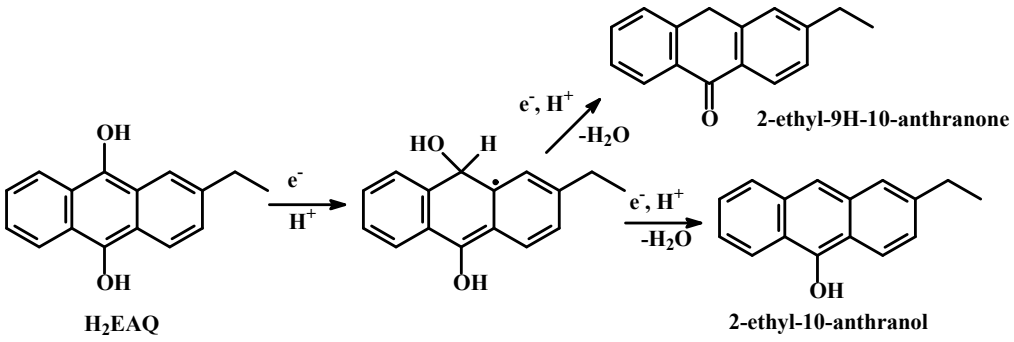

Scheme S2. Possible generation pathway of 2-ethyl-10-anthranol and 2-ethyl-9H-10-anthranone.

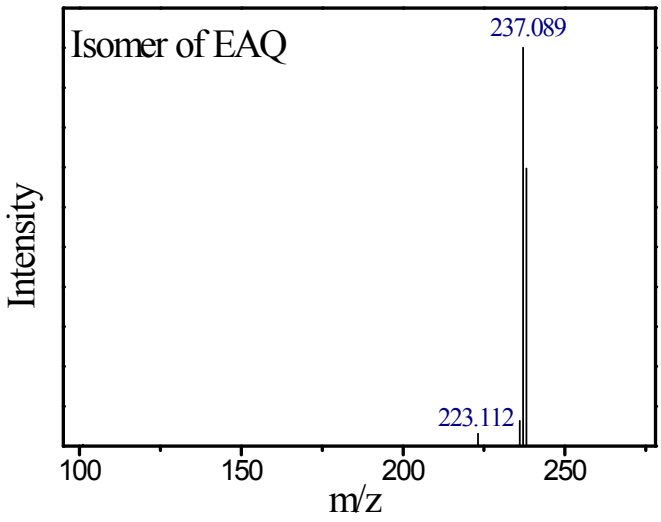

Figure S12. MS spectrum of the substance at retention time of 20.41 min.

MS spectrum of the substances at retention time of 20.41 min is shown in Fig. S12, which has a $[M+H]^+$ signal at m/z 237.089. According to isotopic information and the exact mass, its molecular formula is concluded as $C_{16}H_{12}O_2$. Presumably, it is an isomer of EAQ. However, due to the lack of fragment information, its exact molecular structure has not been identified.

References:

[S1] O. Sekiguchi, V. Bakken, E. Uggerud, Decomposition of Protonated Formic Acid: One Transition State—Two Product Channels. *Journal of the American Society for Mass Spectrometry*, 2004, **15**, 982-988.

[S2] P. R. Boshier, N. Marczin, G. B. Hanna, Repeatability of the Measurement of Exhaled Volatile Metabolites Using Selected Ion Flow Tube Mass Spectrometry. *Journal of the American Society for Mass Spectrometry*, 2010, **21**, 1070-1074.

[S3] H. Prakash, S. Mazumdar, Direct Correlation of the Crystal Structure of Proteins

with the Maximum Positive and Negative Charge States of Gaseous Protein Ions Produced by Electrospray Ionization. *Journal of the American Society for Mass Spectrometry*, 2005, **16**, 1409-1421.

[S4] C. J. Krusemark, B. L. Frey, P. J. Belshaw, et al., Modifying the Charge State Distribution of Proteins in Electrospray Ionization Mass Spectrometry by Chemical Derivatization. *Journal of the American Society for Mass Spectrometry*, 2009, **20**, 1617-1625.

[S5] C. Zhao, T. D. Wood, S. Bruckenstein, Shifts in Protein Charge State Distributions with Varying Redox Reagents in Nanoelectrospray Triple Quadrupole Mass Spectrometry. *Journal of the American Society for Mass Spectrometry*, 2005, **16**, 409-416.

[S6] R. Arakawa, T. Yamaguchi, A. Takahashi, et al., Identification of Face-to-Face Inclusion Complex Formation of Cyclodextrin Bearing an Azobenzene Group by Electrospray Ionization Mass Spectrometry. *Journal of the American Society for Mass Spectrometry*, 2003, **14**, 1116-1122.